Applied Physics
Express

LETTER • OPEN ACCESS

Self-assembled GaAs quantum dashes for direct alignment of liquid crystals on a III–V semiconductor surface

To cite this article: Hugo Villanti *et al* 2025 *Appl. Phys. Express* **18** 027001

OPEN ACCESS

Applied Physics Express 18, 027001 (2025) LETTER

https://doi.org/10.35848/1882-0786/adb3eb

Self-assembled GaAs quantum dashes for direct alignment of liquid crystals on a III–V semiconductor surface

Hugo Villanti[1], Sébastien Plissard[1], Jean-Baptiste Doucet[1], Alexandre Arnoult[1], Benjamin Reig[1], Laurent Dupont[2], and Véronique Bardinal[1*]

[1]LAAS-CNRS, Université de Toulouse, CNRS, 7 Avenue du Colonel Roche, 31400 Toulouse, France
[2]Optics department, IMT Atlantique Technopôle Brest-Iroise CS 83818 29238 Brest cedex 03, France

*E-mail: bardinal@laas.fr

Received December 19, 2024; revised January 13, 2025; accepted February 6, 2025; published online February 25, 2025

The development of tunable photonic devices is strategic for miniaturized optical instrumentation and sensing systems. Exploiting the birefringence variation of liquid crystals (LCs) instead of MEMS actuation in such devices could bring better spectral stability and lower power consumption. However, aligning LCs inside a III–V semiconductor device is tricky. We demonstrate that self-assembled gallium arsenide (GaAs) quantum dashes (QDHs) could serve as direct planar aligners for LC nematic molecules. The alignment quality and birefringence variation of a LC-microcell embedding QDHs are shown to be similar to those of a polymer nanograting-based reference, with the added advantage of better electrical performance. © 2025 The Author(s). Published on behalf of The Japan Society of Applied Physics by IOP Publishing Ltd

Supplementary material for this article is available online

Spectrally-tunable photonic devices such as tunable vertical-cavity surface-emitting lasers (VCSELs) and tunable photodetectors are key elements for the development of compact optical instrumentation and sensing systems,[1)] whether for gas detection,[2)] biomedical imaging,[3)] Bragg grating fiber detection[4)] or miniature spectroscopy. The most mature approach to produce tunable microcavity devices involves adding a moving electromechanical element (MEMS) above the III–V semiconductor active region.[2–7)] However, this can present drawbacks for some applications due to inherent mechanical vibrations in the MEMS.[8,9)] Exploiting the birefringence variation in a liquid crystal intracavity layer[10,11)] could be a promising alternative, as this "no-moving part" solution is likely to provide better wavelength reproducibility and for lower applied voltages (~10–25 V) than those typically involved in electrostatically-actuated MEMS (~80 V). This liquid crystal (LC)-based approach is also of great interest for the dynamic control of polarization properties in VCSELs sources.[12,13)] However, managing LC molecules inside an optical microcavity device is tricky. In particular, the LC alignment technique employed must be compatible with integration on a non-planar surface. Conventional methods generally used in LC-displays, such as polyimide rubbing or UV polarized photo-alignment, are not easily applicable. Another solution consists in orienting the LC molecules along the nanogrooves of a grating.[14–16)] In previous works, the authors developed a LC microcell (μ-cell) technology based on such alignment using a nanoimprinted polymer grating.[17)] This hybrid approach was successfully employed to demonstrate high finesse LC-filters and LC-InP photodiodes tunable over more than 80 nm around 1.55 μm.[18)] We also reported an optically-pumped LC-VCSEL operating at room temperature in a continuous wave regime with a tuning range of 33 nm.[19,20)] However, it is not possible to fabricate individualizable devices to be separately mounted and controlled using this hybrid technology. Moreover, despite several theoretical designs proposed,[12,21,22)] the demonstration of an electrically-driven, LC-tunable VCSEL remains a great challenge.

In this work, we propose to evaluate a new way for LC alignment that would eliminate the need for using an organic alignment layer and therefore help to overcome these obstacles. We show indeed that self-assembled GaAs quantum dashes (QDHs) can directly serve as planar aligners for nematic LC molecules. These III–V semiconductor nanostructures are unstrained quantum dots (QDs) fabricated on GaAs by droplet epitaxy and thermally-elongated to become oriented dashes.[23)] It is worth noting that we propose here to exploit the structural anisotropy of GaAs QDHs and not, as in most works reported up to now, their specific emission properties for optical/quantum applications. They would be transparent at the working wavelength envisioned for the LC-devices and their role would be solely to act as a self-built III–V alignment layer grown within the same epitaxial step than of the device's active region. In this letter, we detail the conditions we have used to fabricate GaAs QDHs suited for LC planar alignment, then describe the μ-cells test samples developed to study the behavior of a nematic LC put in contact with a QDHs surface and to compare it a reference based on a SU-8 nanograting. Finally, experimental results are discussed and compared with optical modeling.

The goal of this study is to evaluate the ability of a III–V self-organized nanopattern to act as an alignment layer for LC molecules. To this aim, self-assembled GaAs QDHs were fabricated on GaAs, starting from unstrained GaAs QDs grown by the droplet epitaxy method.[24)] Growth and post-growth annealing conditions were optimized to elongate the dots along the [−110] crystallographic axis, taking advantage of the anisotropy of the step energy at the surface and drawing inspiration from works reported on the low temperature emission enhancement of such QDs.[23,25)] 2 inch GaAs (001) N-doped wafers from AXT were loaded in a RIBER MBE412 growth chamber. A 100 nm GaAs buffer layer followed by a 100 nm $Al_{0.35}Ga_{0.65}As$ layer were grown at 580 °C and under 1.2×10^{-5} and 1.9×10^{-5} Torr As_4 fluxes, respectively. The substrate temperature was then ramped down to 300 °C under 1.9×10^{-5} Torr As_4 flux for

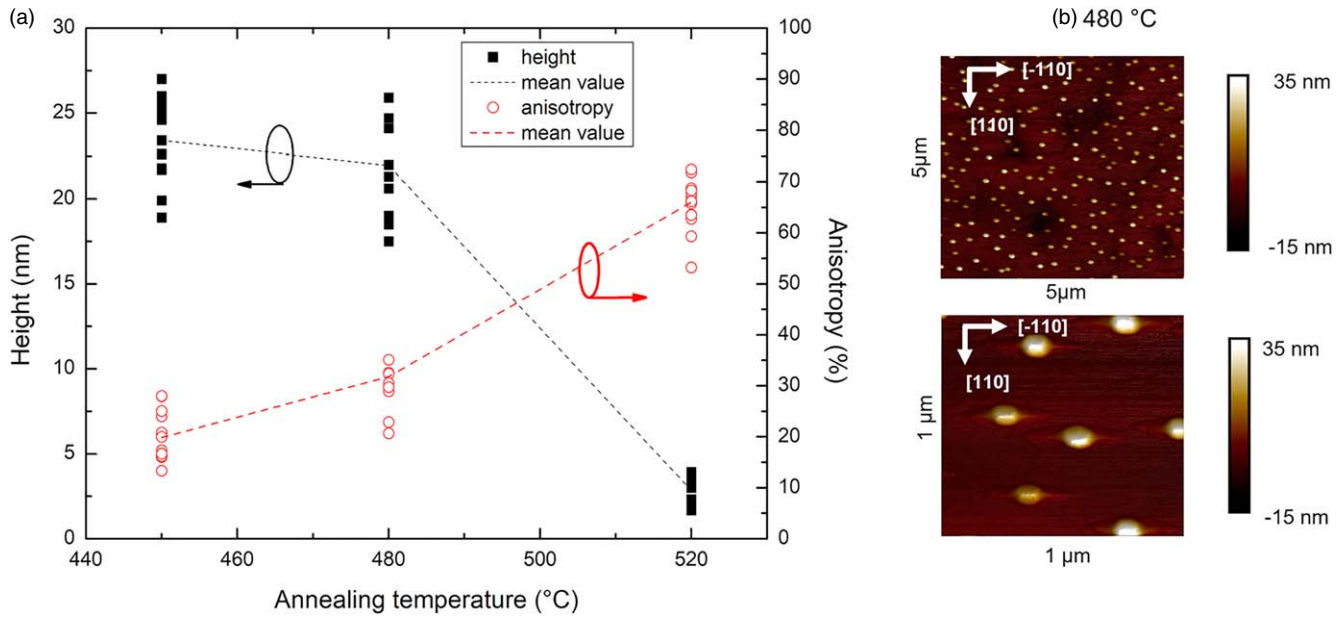

Fig. 1. (a) Measurement of the height (solid black squares) and anisotropy factor (open red circles) of the GaAs QDHs as a function of the annealing temperature (measured at 5 positions on the 2 inch wafer/dotted line: average values). (b) AFM images of the selected QDHs (480 °C, height: 21.94 nm, length: 141.94 nm, width: 101.97 nm, anisotropy: 28%) acquired on $5 \times 5\ \mu m^2$ (top) and $1 \times 1\ \mu m^2$ (bottom) surfaces. (Note that AFM measurements were also taken at 45° to the direction of these images to check the absence of artifact).

temperature above 450 °C and 5 monolayers of Ga were deposited. The temperature was then cooled down to 200 °C for crystallization of the metallic droplets under 2.7×10^{-5} Torr As_4 flux, giving birth to GaAs QDs. Finally, a thermal annealing of the uncapped dots was carried out for 10 min under an As_4 flux of 1×10^{-5} Torr to obtain QDHs. The QDHs' anisotropy factor was defined as the relative difference in length along their long axis ([−110] direction) and short axis ([110] direction) measured from atomic force microscopy (AFM) scans performed on several points on the 2 inch wafer. As shown in Fig. 1(a), this anisotropy reached more than 65% for an annealing at 520 °C, but at the cost of a strong decrease of the QDHs' maximal height (from more than 25 nm to less than 3 nm). As a relief of at least 10 nm is necessary for LC molecules alignment,[16] a trade-off was made on the annealing temperature. For 480 °C, we obtained an average maximal height of 21.94 nm, with a standard deviation of ±2.83 nm over the 2 inch wafer. As illustrated in the corresponding AFM images in Fig. 1(b), the QDHs' density was of the order of 5–10 units per μm^2, which can approximate the density of lines of a submicron period grating already proven for LC alignment in several hybrid tunable LC-devices.[18–20] The question raised was whether the anisotropy factor of these QDHs, namely 28 ± 5%, would be high enough for LC alignment.

Figure 2(b) shows a schematic view of the nematic LC µ-cell fabricated to investigate the feasibility of LC alignment on GaAs QDHs. As seen in Fig. 2(a), a reference sample was also prepared for comparison purposes. This latter relied on a 200 nm period grating (duty cycle: 50%, depth of grooves: 48 nm) printed by T-UV-NIL (thermal UV nanoimprint lithography) in a thin SU-8 photoresist layer previously deposited by spin-coating on the substrate. The choice of a SU-8 nanograting for the reference µ-cell was motivated by the fact it was successfully used for the demonstration of several hybrid LC-tunable III–V devices.[18–20] This approach is indeed simple to apply once the NIL soft mould has been fabricated. It also presents the advantage of not releasing impurities and static electricity at the surface as in the case of polyimide rubbing, nor requiring the use of a specific AZO-dye layer and polarized light as in the case of photoalignment process. More details on the process used can be found in Ref. 17. For both samples, the µ-cells' walls were defined through a mask by standard UV photolithography in a thick negative photoresist having specific adhesive properties (Microchem/Perminex®) and also deposited by spin-coating (thickness ∼3.45 µm). After the walls' development, all µ-cells were sealed at the same time by soft thermal printing at 150 °C of a top cover glass substrate including an ITO (indium tin oxide) transparent electrode (PGO-CEC020Q, 20 ohm $square^{-1}$). The µ-cells were then filled under vacuum at 110 °C by capillary effect with a liquid crystal material similar to BLC036 from Merck ($QYPDLC\text{-}36/V_{90\text{–}20C} = 2.247$ V).[26] This LC material has a high clarification temperature (95 °C) that is well suited for insertion in an active photonic device.[27] It is worth noting that we did not add a second alignment layer on the opposing face of the µ-cell (i.e. on the top ITO internal face), as we showed in previous works that the use of a single grating was sufficient to ensure LC alignment in a device with a LC thickness lower than 5 µm.[17–19] The only difference between the two samples lied in the nature of the alignment layer tested, namely a SU-8 nanograting for the first case (Fig. 2(a)) and an array of GaAs QDHs grown on a buffer composed of a 100 nm thick GaAs layer and a 100 nm thick $Al_{0.35}Ga_{0.65}As$ layer for the second one (Fig. 2(b)).

Figure 3(a) shows three images of the µ-cells' surface acquired with an optical microscope (x20) between crossed polarizers and for different angles (45°, 25° and 0°) between the polarizer axis and the LC alignment direction, represented by a white arrow. This latter corresponds to the mean axis of the LC's director ($\hat{n}$). It should be noted that due to the deposition technique used (spin-coating), the uncertainties in

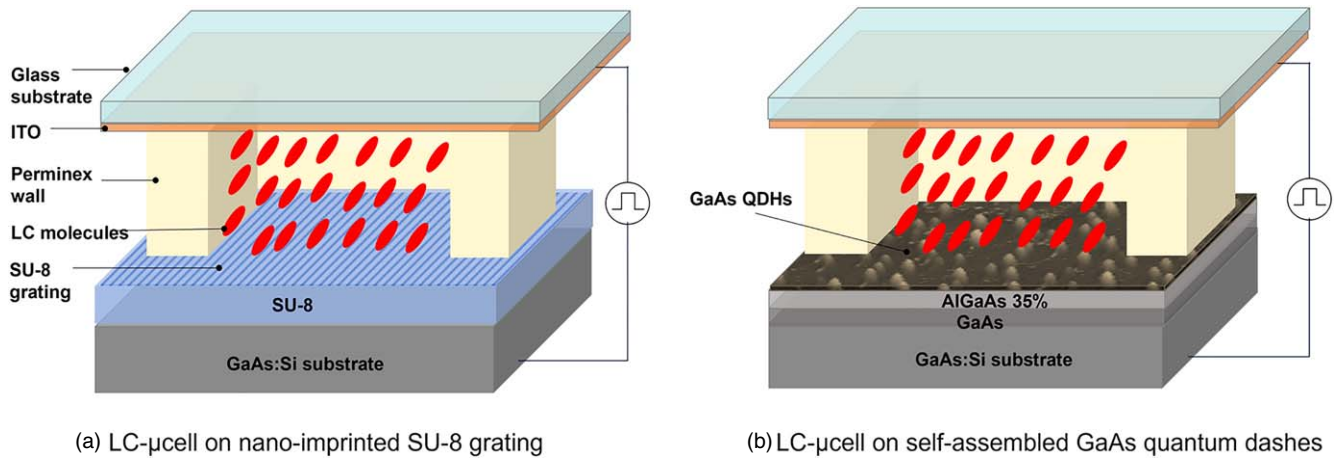

Fig. 2. Schematic cross view of LC µ-cells fabricated on a N-doped GaAs substrate: (a) with a reference SU-8 nanograting (period: 200 nm/groove depth: 48 nm/duty cycle: 50%, SU-8 layer; 700 nm) (b) with GaAs QDHs (height ∼22 nm, anisotropy ∼28%, density: ∼7 QDHs µm^{-2}). The area of each µ-cell is 2, 8 × 2, 8 mm^2.

the thicknesses of the organic layers present in both samples (i.e. the polymer walls height, plus the SU-8 thickness for the reference µ-cell) were large (±0, 1 µm). To enable a rigorous comparison, we selected for this study only µ-cells having the same walls' height before sealing (measured by mechanical profilometry) and the same initial surface color observed between cross-polarizers after LC filling, thus guaranteeing the same LC thickness (3.45 µm). As can be seen in Fig. 3(a), the surface of the µ-cell enclosing the SU-8 grating reflected homogeneously a maximum amount of light when the director $\hat{n}$ was oriented at 45° to the analyzer axis. As the angle decreased, an intermediate state appeared, followed by a total extinction when $\hat{n}$ was parallel to the analyser axis. This is the angular behavior expected for a standard LC cell. We observed a similar result for the QDHs-based µ-cell, with a quite homogeneous texture and a gradual change, from high intensity to a state of extinction when the angle was varied from 45° to 0°, as expected. This indicates that the GaAs QDHs did act as planar alignment guides for the LC molecules, which seemed to see the QDHs as almost infinite lines despite their limited length. We account this to the small size of the LCs (typical length∼3 nm) and to a collective alignment effect.

The angular evolution of the reflected signal was measured over a wider range and by inserting a narrow band pass filter in the optical path of the microscope's white light source to filter the signal (FWHM: 1 nm @ 696 nm). As shown in Fig. 3(b), for both cases, a periodic change in intensity was observed for intervals of 90°, as aimed (Fig. 3 (b)). The extinction contrast measured for the QDHs µ-cell was only slightly lower. This is accounted to the fact the height of the grating grooves was around 2 times higher than the QDHs' height, probably leading to a small difference in the azimuthal anchoring energy.[16] It is important to note that it is possible to further optimize the QDHs height by playing more finely on the droplet epitaxy conditions. Nevertheless, these first results clearly indicate that the height of the QDHs tested is already enough to ensure a LC alignment.

The electro-optical behavior of the LC µ-cells was then studied by observing the evolution of the cell surface as a function of the AC voltage applied between the bottom (n-doped GaAs) and bottom (ITO) electrodes. This was first carried out between crossed polarizers under white light illumination. A synthetic view of the image sequences acquired for applied voltages ranging from 0 to 18 V is presented in Fig. 4 (see details in Supplementary material #1). As seen, the surface color started

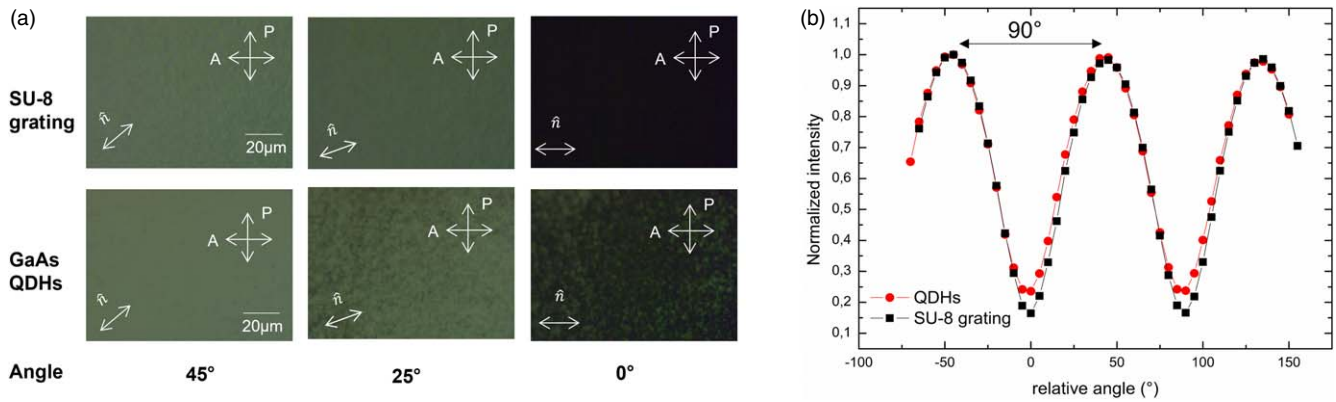

Fig. 3. (a) Images of the cells' surface observed with an optical microscope (reflection mode, X20, white light illumination) between crossed polarizers for 3 different angles between the LC director and the analyser axis (45°, 25° and 0°): (top) SU-8 µ-cell, (bottom) QDHs µ-cell. (b) Normalized reflected light measured as a function of the angle for the SU-8 grating µ-cell (black squares) and for the QDHs µ-cell (red circles) (reflection mode, X20, white light filtered with a 696 nm narrow band optical filter).

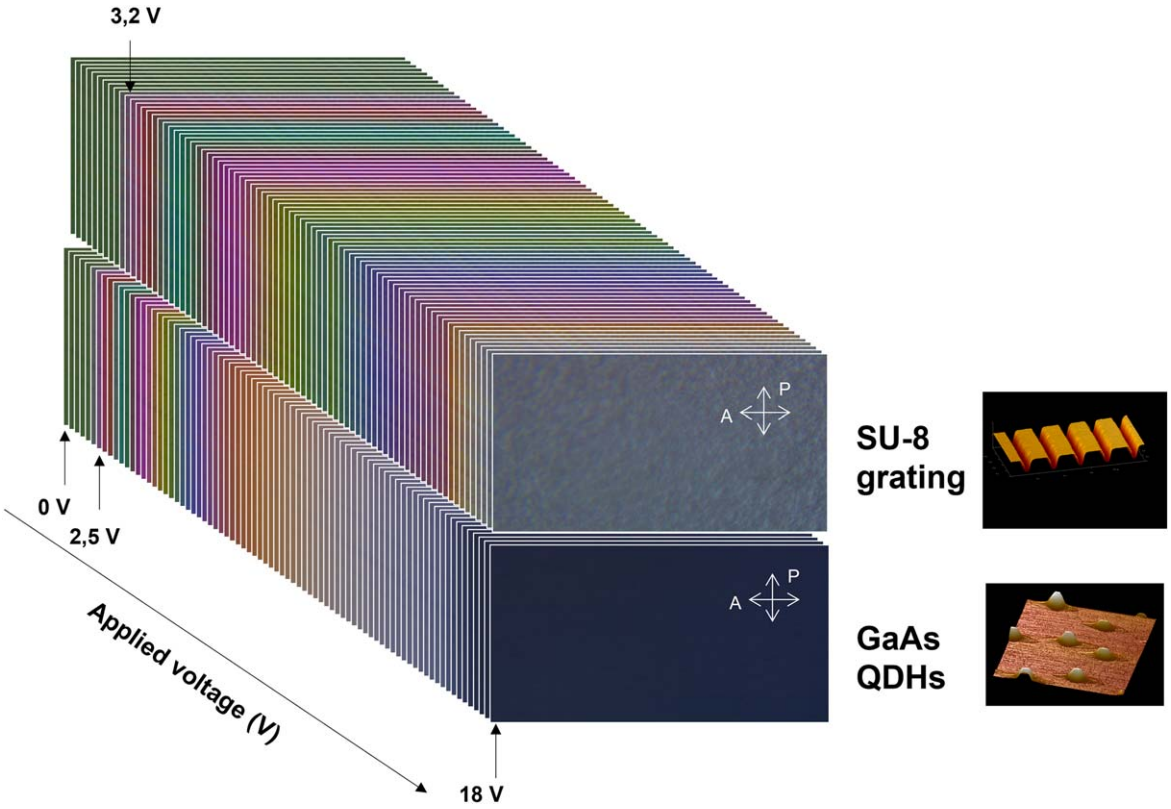

Fig. 4. Images sequences of the surfaces acquired as a function of the external voltage applied (2 kHz Steps^{-1}: 1 V between 0 and 2 V, 0, 1 V between 2, 5 V and 9 V and 1 V between 9 V and 18 V) for the SU-8 grating (top) and QDHs (bottom) μ-cells (reflection mode, X20, white light, crossed polarizers, LC director at 45° to the polarizers) Insets: 3D AFM images of the SU-8 grating (0.5 × 1 μm^2) and GaAs QDHs (1 × 1 μm^2) surfaces.

to vary above 2.5 V, respectively 3.2 V, for the QDHs μ-cell, respectively the SU-8 μ-cell. Above this threshold indicating the beginning of the LC orientation variation, successive color changes following the same order were observed in both cases, showing that the phase variation was similar in the two μ-cells. Nevertheless, the corresponding external voltage to apply was found much lower for the QDHs μ-cell case, suggesting a better electrical behavior. For example, a totally black surface could be observed for the maximal voltage (18 V), compared to only a dark gray one for the SU-8 grating μ-cell under the same conditions.

To make a more quantitative analysis possible, we acquired new images stacks with the narrow band visible filter inserted in the optical path of the polarized microscope. The corresponding evolution of the filtered reflected intensity is plotted as a function of the applied voltage in Fig. 5(a). For both cases, an oscillatory signal could be observed above threshold, as expected from the literature.[28,29] To check whether the number of oscillations seen was in good agreement with the aimed variation in birefringence, we calculated the theoretical evolution of the reflectivity at the observation wavelength (696 nm), using an optical modeling tool based on a matrix formalism that takes into account the indices and thickness of all the layers present in each stack.[30] This calculation was carried out assuming the LC birefringence equal to the maximal possible at the considered wavelength (Δn @ 696 nm = 0.24).[27] As we had no access to the effective non-linear dependence of the LC index on the applied voltage, we assumed a simple linear decrease, from the maximal value, $n_e = 1.77$ (extraordinary index value at 696 nm) to the minimal one, $n_o = 1.53$ (ordinary index value at 696 nm) applying a constant step of −0.1 (Fig. 5(b)). In addition, taking into account the uncertainties on the organic layer's thicknesses (LC and SU-8), we tested several values for the LC thickness within the possible variation range [3.35–3.55 μm] and first simulated the case of the QDHs μ-cell (see details in Supplementary material #2). The best agreement with the experimental curve shape was obtained for 3.45 μm [see red curve in Fig. 5(b)], which is in line with the thickness measurement made before μ-cell sealing. Setting the same LC thickness for the SU-8 grating μ-cell, we then tested several thicknesses for the SU-8 layer in the possible range [600–800 nm] and found also a good match for the expected value (700 nm) [see black curve in Fig. 5(b)]. Most importantly, whatever the values tested in possible thickness ranges, the simulation predicted always the observation of almost 2.5 complete oscillations, as seen in our experiments. This demonstrates that in both μ-cells, a complete rotation of the LC director was achieved, from a planar to a homeotropic state.

In addition, as previewed in Fig. 4, the measured voltages at which the extrema appeared were confirmed to be much lower for the QDHs μ-cell than for the SU-8 grating one. This better behavior can be attributed to the fact that, in a thin LC-cell (<5 μm), the actual voltage applied to the LC layer is known to depend not only on the LC's characteristics but also of the nature of the alignment layer.[31] As the dielectric constant of GaAs is much higher than that of SU-8 ($\varepsilon_{GaAs} \sim 13$ compared to $\varepsilon_{SU\text{-}8} \sim 3$), a higher effective field is therefore expected to be applied in the QDHs case. This can be also resulting from a more favorable electrical access configuration, as the undoped buffer located beneath the QDHs is only 200 nm thick, to be compared to 700 nm of insulating SU-8 layer in the reference μ-cell. Note that the

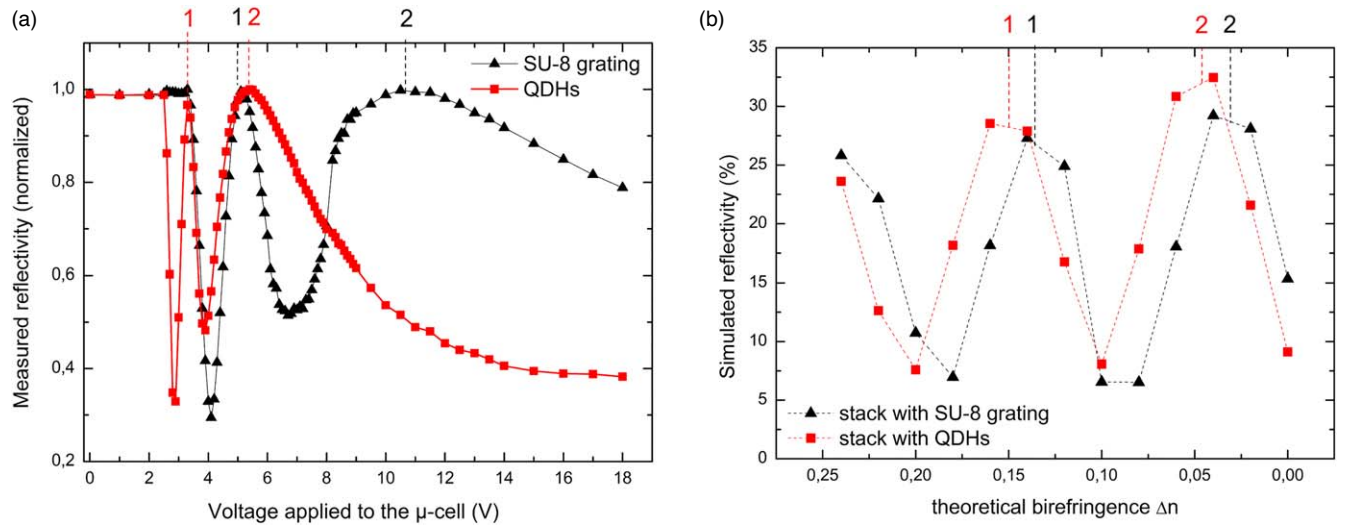

Fig. 5. (a) Measurement of the filtered reflectivity of the SU-8 grating μ-cell (black open squares) and QDHs μ-cell (red solid circles) as a function of the AC voltage applied filter. (b) Simulation of the reflectivity at 696 nm of each μ-cell stack versus the expected LC birefringence variation above threshold (assuming a linear decrease, from 0.24 to 0, a LC thickness of 3.45 μm and a SU-8 thickness of 700 nm). At least 2 maxima are expected to be seen for both stacks, as observed in the experiments.

SU-8 thickness cannot be easily reduced due to spin-coating limitations, whereas the thin epitaxial buffer layers below the QDHs could be also doped in the future, further reducing the stack resistivity. The part of the external voltage applied to the LC layer was estimated theoretically for both cells using the straightforward formula given in Ref. 31 and adapting it to the case of a single alignment layer. We found a voltage ratio between the two cells of ∼1.9, which is of the same order of magnitude as in our experimental observations under high field (∼2.1). Finally, as already mentioned, a small difference in the pre-tilt angle and/or the anchoring energy can also contribute to this more efficient electrooptic behavior. Future work will consist in precisely measuring these parameters as a function of the height of the QDHs to settle this question. Impedance measurements will be also performed to build an equivalent circuit model and quantify more precisely the contribution in electrical efficiency brought by an alignment via the QDHs.[32] In any case, we can already conclude that LC-III–V devices that will rely on GaAs QDHs for LC alignment will exhibit a similar birefringence tunability than their counterparts integrating a SU-8 nanograting, with the additional advantage of better electrical performance.

In conclusion, the feasibility of directly aligning a nematic LC material along self-assembled QDHs grown on a GaAs substrate has been demonstrated. The angular behavior of a LC μ-cell incorporating these anisotropic III–V nanostructures was compared to that of a reference relying on a polymer nanograting. Similar alignment quality was obtained, as well as an optical behavior in line with modeling, and moreover for an applied voltage to apply around 25% lower than for the reference. Future work will consist in integrating these GaAs QDHs aligners into III–V active devices, such as an optically-pumped LC-VCSEL with improved tuning performances, as well as a monolithic device grown within a single epitaxial sequence followed by a localized sacrificial etching for the LC cavity opening. This will enable the fabrication of individually addressable and electrically-controlled LC-photodiodes and LC-VCSELs with a higher degree of flexibility. Finally, the development of this "bottom-up" alignment approach is fully in line with a global research effort currently aimed at aligning LCs on nanostructured surfaces with no organic layer nor costly ITO electrodes[29,33,34] and could be a gateway for the design of other kinds of LC electro-optical devices.

Acknowledgments Agence Nationale de la Recherche (ANR) (Grant Nos.: ANR-15-CE19-0012 DOCT-VCSEL and ANR-20-CE24-0020 3D-BEAM-FLEX). This study benefited from the support of the LAAS-CNRS micro and nanotechnologies platform, member of the French RENATECH network. The authors acknowledge Richard Monflier at LAAS-CNRS for his help on characterization, as well as Christophe Levallois and Cyril Paranthoën at FOTON Institute Rennes, France for fruitful discussions.

Disclosure

The authors declare no conflicts of interest.

ORCID iDs Sébastien Plissard https://orcid.org/0000-0002-0769-5429
Alexandre Arnoult https://orcid.org/0000-0001-8240-8269
Laurent Dupont https://orcid.org/0000-0003-1355-7871
Véronique Bardinal https://orcid.org/0000-0001-9242-4457

1) B. D. Padullaparthi, J. Tatum, and K. Iga, *VCSEL Industry: Communication and Sensing* (Wiley, New York, 2021).
2) B. Kogel, H. Halbritter, S. Jatta, M. Maute, G. Bohm, M. C. Amann, and P. Meissner, IEEE Sens. J. **7**, 1483 (2007).
3) D. D. John, C. B. Burgner, B. Potsaid, M. E. Robertson, B. K. Lee, W. J. Choi, and V. Jayaraman, J. Lightwave Technol. **33**, 3461 (2015).
4) T. Mizunami, T. Yamada, and S. Tsuchiya, Opt. Rev. **23**, 703 (2016).
5) C. J. Chang-Hasnain, IEEE J. Sel. Top. Quantum Electron. **6**, 978 (2000).
6) P. Qiao, K. Cook, K. Li, and C. J. Chang-Hasnain, IEEE J. Sel. Top. Quantum Electron. **23**, 1700516 (2017).
7) A. Simonsen, M. Payandeh, S. E. Hansen, A. Marchevsky, G. C. Park, H. K. Sahoo, E. Semenova, O. Hansen, and K. Yvind, Opt. Lett. **49**, 802 (2024).
8) H. Halbritter, C. Sydlo, B. Kogel, F. Riemenschneider, H. L. Hartnagel, and P. Meissner, IEEE J. Sel. Top. Quantum Electron. **13**, 367 (2007).
9) B. Johnson, J. Jabbour, M. Malonson, E. Mallon, S. Woo, T. Ford, N. Kemp, and P. Whitney, Opt. Express **30**, 17230 (2022).
10) O. Castany, L. Dupont, A. Shuaib, J. P. Gauthier, C. Levallois, and C. Paranthoën, Appl. Phys. Lett. **98**, 161105 (2011).
11) J. Mysliwiec, A. Szukalska, A. Szukalski, and L. Sznitko, Nanophotonics **10**, 2309 (2021).

12) L. Frasunkiewicz, T. Czyszanowski, H. Thienpont, and K. Panajotov, Opt. Commun. **427**, 271 (2018).
13) Y. Dai, L. Shi, Y. Song, Y. Zou, J. Fan, X. Fu, and X. Ma, Opt. Express **32**, 40755 (2024).
14) D. W. Berreman, Phys. Rev. Lett. **28**, 1683, (1972).
15) H. Takahashi, T. Sakamoto, and H. Okada, J. Appl. Phys. **108**, 113529 (2010).
16) C. Gear, K. Diest, V. Liberman, and M. Rothschild, Opt. Express **23**, 807 (2015).
17) B. Sadani, B. Boisnard, X. Lafosse, T. Camps, J. B. Doucet, E. Daran, and V. Bardinal, IEEE Photonics Technol. Lett. **30**, 1388 (2018).
18) C. Levallois, B. Sadani, B. Boisnard, T. Camps, C. Paranthoen, S. Pes, and V. Bardinal, Opt. Express **26**, 25952 (2018).
19) B. Boisnard et al., IEEE Photonics Technol. Lett. **32**, 391 (2020).
20) C. Paranthoen et al., "33 nm wavelength tuning of a 1550 nm VCSEL," 2021 27th Int. Semiconductor Laser Conf. (ISLC), Potsdam, Germany, 2021, p. 1, doi:10.1109/ISLC51662.2021.9615666.
21) C. Belmonte, L. Frasunkiewicz, T. Czyszanowski, H. Thienpont, J. Beeckman, K. Neyts, and K. Panajotov, Opt. Express **23**, 15706 (2015).
22) P. Debernardi, A. Simaz, A. Tibaldi, B. Boisnard, T. Camps, F. Bertazzi, and V. Bardinal, IEEE J. Sel. Top. Quantum Electron. **28**, 1 (2021).
23) M. Jo, T. Mano, and K. Sakoda, Appl. Phys. Express **3**, 045502 (2010).
24) S. Sanguinetti, S. Bietti, and N. Koguchi, "Droplet epitaxy of nanostructures," *Molecular Beam Epitaxy* (Elsevier, Amsterdam, 2018) p. 293.
25) S. Adorno, S. Bietti, and S. Sanguinetti, J. Cryst. Growth **378**, 515 (2013).
26) https://canaanchem.com/.
27) A. Simaz, B. Boisnard, J. B. Doucet, T. Camps, B. Reig, J. Lumeau, and V. Bardinal, Opt. Mater. Express **12**, 383 (2022).
28) L. M. Blinov et al., *Electrooptic Effects in Liquid Crystal Materials* 1994) p. 133.
29) R. Basu, Appl. Phys. Lett. **123**, 090501 (2023).
30) H. A. Macleod, *Thin-film Optical Filters* (CRC Press, Boca Raton, 2018).
31) M. Jiao, Z. Ge, Q. Song, and S-T. Wu, Appl. Phys. Lett. **92**, 061102 (2008).
32) A. Abderrahmen, F. F. Romdhane, H. B. Ouada, and A. Gharbi, Sci. Technol. Adv. Mater. **9**, 025001 (2008).
33) P. Blake, P. D. Brimicombe, R. R. Nair, T. J. Booth, D. Jiang, F. Schedin, and K. S. Novoselov, Nano Lett. **8**, 1704 (2008).
34) P. Priscilla, P. Malik, Supreet, A. Kumar, R. Castagna, and G. Singh, Crit. Rev. Solid State Mater. Sci. **48**, 57 (2022).